

Epidermal Inorganic Optoelectronics for Blood Oxygen Measurement

Haicheng Li, Yun Xu, Xiaomin Li, Ying Chen, Yu Jiang, Changxing Zhang, Bingwei Lu, Jian Wang, Yinji Ma, Yihao Chen, Yin Huang, Minguang Ding, Honghong Su, Guofeng Song, Yi Luo, and X. Feng*

Flexible and stretchable optoelectronics, built-in inorganic semiconductor materials, offer a wide range of unprecedented opportunities and will redefine the conventional rigid optoelectronics in biological application and medical measurement. However, a significant bottleneck lies in the brittleness nature of rigid semiconductor materials and the performance's extreme sensitivity to the light intensity variation due to human skin deformation while measuring physical parameters. In this study, the authors demonstrate a systematic strategy to design an epidermal inorganic optoelectronic device by using specific strain-isolation design, nanodiamond thinning, and hybrid transfer printing. The authors propose all-in-one suspension structure to achieve the stretchability and conformability for surrounding environment, and they propose a two-step transfer printing method for hybrid integrating III–V group emitting elements, Si-based photodetector, and interconnects. Owing to the excellent flexibility and stretchability, such device is totally conformal to skin and keeps the constant light transmission between emitting element and photodetector as well as the signal stability due to skin deformation. This method opens a route for traditional inorganic optoelectronics to achieve flexibility and stretchability and improve the performance of optoelectronics for biomedical application.

epidermal devices,^[11–13] with the distinct ability compared to traditional electronics, are subjected to synchronous deformation with skin and own the comprehensive capability of bending, stretching, and twisting.^[14,15] However, conventional optoelectronic devices based on light detection are extremely sensitive to light intensity or phase variation due to displacement or deformation.^[16] For instance, skin deformation or body motion exerts the unpredictable influence on optical path of light beam in current commercial oximeter, as a result, the photoplethysmography (PPG) signal is seriously disturbed.^[17,18] Thus, currently optoelectronic device is inappropriate to quantitatively detect blood oxygen in usual life besides its inconvenience of rigidity. In order to achieve both medical precision measurement and mechanical invisibility to skin motion, epidermal optoelectronic devices have to own excellent flexibility and stretchability, which requires special structure and fabrication technique for optimal optical design.

Transfer printing technique^[19–22] is commonly utilized in flexible electronics fabrication to set the elements defined on the donor wafer to the targeted soft substrate. However, epidermal optoelectronics, possessing light emitting and detecting ability are confronted to heterogeneous integration of functional elements from different substrates such as III–V group or silicon. Also, for optimizing

1. Introduction

Epidermal or E-skin devices,^[1–5] naturally conformal and compatible to objects (e.g., skin) with unusual geometry, offer an opportunity for widespread applications such as long-term and continuous physiological monitoring.^[6–10] Multifunctional

H. Li, Y. Chen, Dr. C. Zhang, Dr. B. Lu, Dr. Y. Ma,
Y. Chen, Dr. Y. Huang, M. Ding, Prof. X. Feng
AML
Department of Engineering Mechanics
Tsinghua University
Beijing 100084, China
E-mail: fengxue@tsinghua.edu.cn

H. Li, Y. Chen, Dr. C. Zhang, Dr. B. Lu, Dr. Y. Ma,
Y. Chen, Dr. Y. Huang, M. Ding, Prof. X. Feng
Center for Mechanics and Materials
Tsinghua University
Beijing 100084, China

DOI: 10.1002/adhm.201601013

Prof. Y. Xu, X. Li, Y. Jiang, Prof. G. Song
Nano-Optoelectronics Laboratory
Institute of Semiconductors
Chinese Academy of Sciences
Beijing 100083, China

Prof. J. Wang, Prof. Y. Luo
National Lab for Information Science and Technology
Department of Engineering
Tsinghua University
Beijing 100084, China

Dr. H. Su
Research and development department
Chero Technology Co., Ltd.
Jiaxing 314001, China



the flexible configuration and performance, several strain isolation techniques are provided for adaptive deformation, by using hybrid rigid-island structure,^[23] ultralow-modulus elastomer,^[24] and microfluidic enclosure.^[25] These techniques are effective in mechanical aspect, yet insufficient in optical design for optoelectronic devices. Thus, for designing and fabricating an epidermal optoelectronic device, the key issues include (1) the optical design for eliminating noise and signal instability caused by the light path disturbance due to deformation, and simultaneously, the structure design for flexibility and stretchability, (2) the low efficiency and success ratio to fabricate ultrathin optoelectronic devices due to the intrinsic brittleness of inorganic optoelectronic materials, (3) the method for heterogeneously integrating optoelectronic devices with different substrate materials.

Here, we demonstrate a systematic strategy to design an epidermal inorganic optoelectronic device by using specific strain-isolation design, nanodiamond thinning technique and hybrid transfer printing. We then fabricate the epidermal optoelectronic devices, which can adhere to skin for blood oxygen measurement based on Beer–Lambert law. In order to keep the optical path unchanged under skin deformation, we propose all-in-one suspension structure for adaptive deformation, and two sequential transfer printing steps for hybrid integrating III–V group emitting elements, Si-based photodetector elements, and interconnects. As a result, the device owns excellent flexibility and stretchability, and adapts to skin deformation whilst maintaining the optical path unchanged. Also, nanodiamond thinning technique is developed to physically thin the prepared element arrays from a few hundred micrometers to $\approx 20 \mu\text{m}$ thickness before transfer printing. Finally, we attach such epidermal optoelectronic devices to the finger and wrist to measure the blood oxygen level respectively, indicating the device's ability to avoid the disturbance of tissue deformation during speaking and arm moving. This demonstrates the affectivity and feasibility of designed epidermal optoelectronic devices for quantitative and precision medical monitoring.

2. Design and Fabrication

Figure 1 illustrates the scenarios, basic principle, and our design of epidermal optoelectronic device via hybrid integration. Compared with traditional devices, epidermal devices are ultrathin, imperceptible, flexible and stretchable, and totally conformal to human body with “mechanical invisible.” Combined light emitting or receiving/detecting elements with different working wavelength, the devices offer different functions when attached to different position of human body. For instance, epidermal optoelectronic device can monitor the brain activity via interaction between light and neurosystem when attached to head, measure the pulse, blood oxygen, and blood pressure via PPG when attached to wrist, and cure the breast cancer via laser when attached to breast, as shown in **Figure 1a**. The light-emitting diodes (LEDs) can be employed for monitoring brain activity, and this epidermal devices have ability to adhere on human breast, and the tumor is long-time and continually exposure by laser. These conceptual applications demonstrate continuous and long-term healthcare and disease treatment via epidermal optoelectronic devices. **Figure 1b** shows the epidermal optoelectronic device is attached to skin and totally conformal to epidermis. Following deformation of human skin (e.g., bending and stretching) in real life, epidermal device adapts to the deformation and does not degrade its performance. Moreover, such device is mechanical invisible to human body and then realizes the long-term working in usual life. Usually, the traditional inorganic optoelectronic device can keep the constant and stable light transmission between emitting elements and detecting elements due to rigidity. However, the situation will be destroyed due to the deformation (i.e., bending or stretching) of epidermal optoelectronic device, because the light path is extremely sensitive to deformation. For example, when we measure the human SpO_2 , we concern the light absorption by hemoglobin and deoxyhemoglobin. However, the light intensity is sensitive to external condition, such as the distance between light emitting and receiving units. When

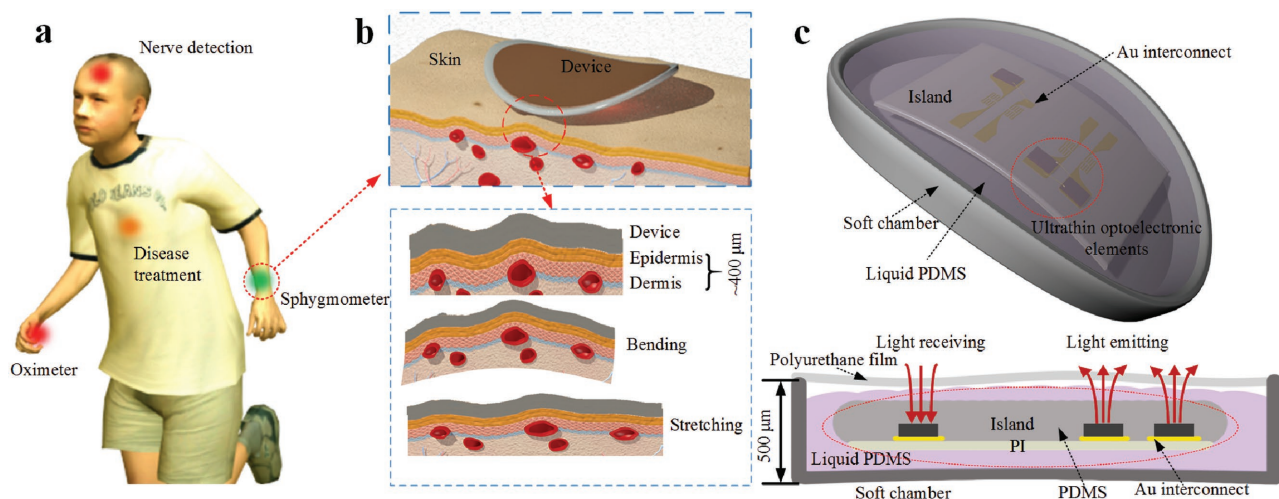


Figure 1. The scenarios, basic principle, and design of epidermal optoelectronic device via hybrid integration. a) A schematic diagram of epidermal optoelectronic devices attached to different positions of human body, including multi-physiological parameters monitoring and disease treatment. b) A zoom-in picture and cross section of the device on skin. c) The illustration of designed all-in-one suspension structure to achieve the stretchability and flexibility.

the epidermal device is adhered on skin and stretched with human skin, the distance between the LEDs and photodetector, as shown in Figure 4. There is a distance shift before and after skin deformation. Thus the light path, which is related to light intensity, has been changed. Therefore, in order to avoid such shortage, we propose a specific structure and fabrication with universal applicability for epidermal optoelectronic device. The proposed device involves three important factors, including all-in-one suspension structure design, nanodiamond thinning technology, and hybrid transfer printing. The idea of all-in-one structure is mainly the adaptive strain isolation by flexible free-suspension island in viscous fluid environment provided by the soft chamber as shown in Figure 1c. The island is composed as sandwich structure of substrate (i.e., polyimide (PI))/function layer/internal encapsulation (Polydimethylsiloxane (PDMS)). The function layer includes light-emitting elements based on GaAs, photodetector based on silicon and Au interconnects, and is located almost in the neutral plane of PI and PDMS. The soft chamber is consist of cured PDMS and semipermeable polyurethane film, both of them is not only flexible and stretchable, but also excellent permeable to invisible and infrared light (up to 95%). Also, the semipermeable polyurethane film is breathable and waterproof, thus this material is comfortable on skin for long-term measurement. Then the liquid PDMS with optical transparency and good dielectric property is used to package the island creating a friendly environment for the functional elements and circuit. When the device is subjected to deformation, such as stretching and bending, the soft chamber with liquid PDMS will absorb the deformation and the island will keep the distances between light-emitting elements and photodetector unchanged. Also, we fabricated wire connections on the suspension island. Thus the wire is also strain isolated and minor deformation occurs in the working state. Thus signal error result from optical path changing during practical measurement on human skin is diminished. The optics transmission in epidermis tissue will be discussed latter.

We fabricate the epidermal device with the all-in-one structure following above design. Figure 2a shows the flow chart of fabrication. The island integrates two ultrathin light emitting elements, i.e., red and infrared LEDs with center wavelength of 620 and 850 nm, respectively, and one ultrathin photodetector element with the spectrum from 400 to 1100 nm. Both red and infrared LED dies are AlGaInP/AlGaAs quantum well structure epitaxial grown on GaAs substrate, photodetector die is fabricated by doping impurity as vertical Gaussian distribution. All the elements are $\approx 20 \mu\text{m}$ with nanodiamond thinning technique, which will be discussed latter. It is fabricated from preparing polymethyl methacrylate (PMMA, 500 nm)/PI (2 μm)/Au (600 nm) are sequentially deposited on a silicon wafer. Photolithography defines the fractal Au interconnects with the width of 50 μm and Au square electrodes (1 \times 1 mm). Then we use stamp-assisted transfer printing technique to place the ultrathin LEDs and Photodetector(PD) to the corresponding pads. Liquid PDMS is spin coated on the top and cured to solid state, which forms as an enclosure. Thus the island including both ultrathin LEDs and PD is realized. And then, liquid transfer printing technique is utilized by undercutting the sacrificial layer to release the island from silicon wafer. A 500 μm thick PDMS chamber molding by aluminum pattern

is filled with uncured PDMS. Therefore, the island structure is immersed in liquid PDMS. Furthermore, the other side of the chamber is encapsulated by polyurethane film. Figure 2b shows the pictures of epidermal optoelectronics device, and insets show two emitting elements are lightened in working status respectively. Figure 2c shows the epidermal optoelectronic device attached to human forefinger.

Thinning technology is adopted and improved to obtain ultrathin and high-performance semiconductor die for applications in flexible electronics. Unlike traditional thinning processing which focus on wafer size device and chemical etching, nanodiamond grinding technique used here, can obtain millimeter-size optoelectronic element arrays with much smaller thickness. Different optoelectronic dies are thinned with this technique and the results is shown in Figure 3. Figure 3a is the scanning electron microscope (SEM) pictures of different thinned optoelectronic elements, including red LED (the first row, 620 nm, GaAs based), infrared LED (the second row, 850 nm, GaAs based) and photodetector (the third row, 400–1100 nm, silicon based). Because nanodiamond thinning is a pure mechanical processing, the thinning die avoids corrosion by chemical reaction (i.e., acid, alkali). Due to limited residual stress, the smaller die is prone to grind extremely thin without any crack. The thickness of the three dies after thinning are 17.78, 26.38, and 20.28 μm , respectively, compared with original 180.2/177.3/301.9 μm , this method for removing substrate of each dies reveal quite efficiency and highlight: up to 90% extra useless substrate diminishes.

Figure 3b shows the spectral properties of the representative ultrathin die. The normalized electroluminescent (EL) of LEDs and absolute spectral responsivity of PD are almost the same before and after thinning. Obviously, such thinning technique does not influence the die properties. This method is appropriate for most semiconductor devices and has advantage of compatibility with traditional semiconductor technology.

3. Optical and Mechanical Simulation

Epidermal optoelectronic devices attached to skin are prone to be affected by skin deformation or body motion. For instance, such devices can detect light intensity variation to monitor physiological parameters, such as blood oxygen. Therefore, the change of light path is considered when the surrounding skin or tissue deforms. In other words, the epidermal optoelectronic device relies on the principle of light scattering in biological tissue. However, based on detecting light scattering strength, light intensity received by photodetector is seriously influenced by the distance between light emitting and receiving source (D_{lp}), as shown in Figure 4a. To obtain the optimized adaptive deformation design of the device, we set up a 2D model for simulating the tissue under epidermis shown in Figure 4b. Numerical Monte Carlo (MC) method^[26–28] is used to calculate photon migration and light scattering path under epidermis. The model and calculation details are available in the Experimental Section. Figure 4c,d illustrates the distribution diagram of photon migration in the tissue and Figure 4d is the enlarged 40 \times 0.8 mm part of subcutaneous tissue. A maximum reflection of light exists near emission source after fully

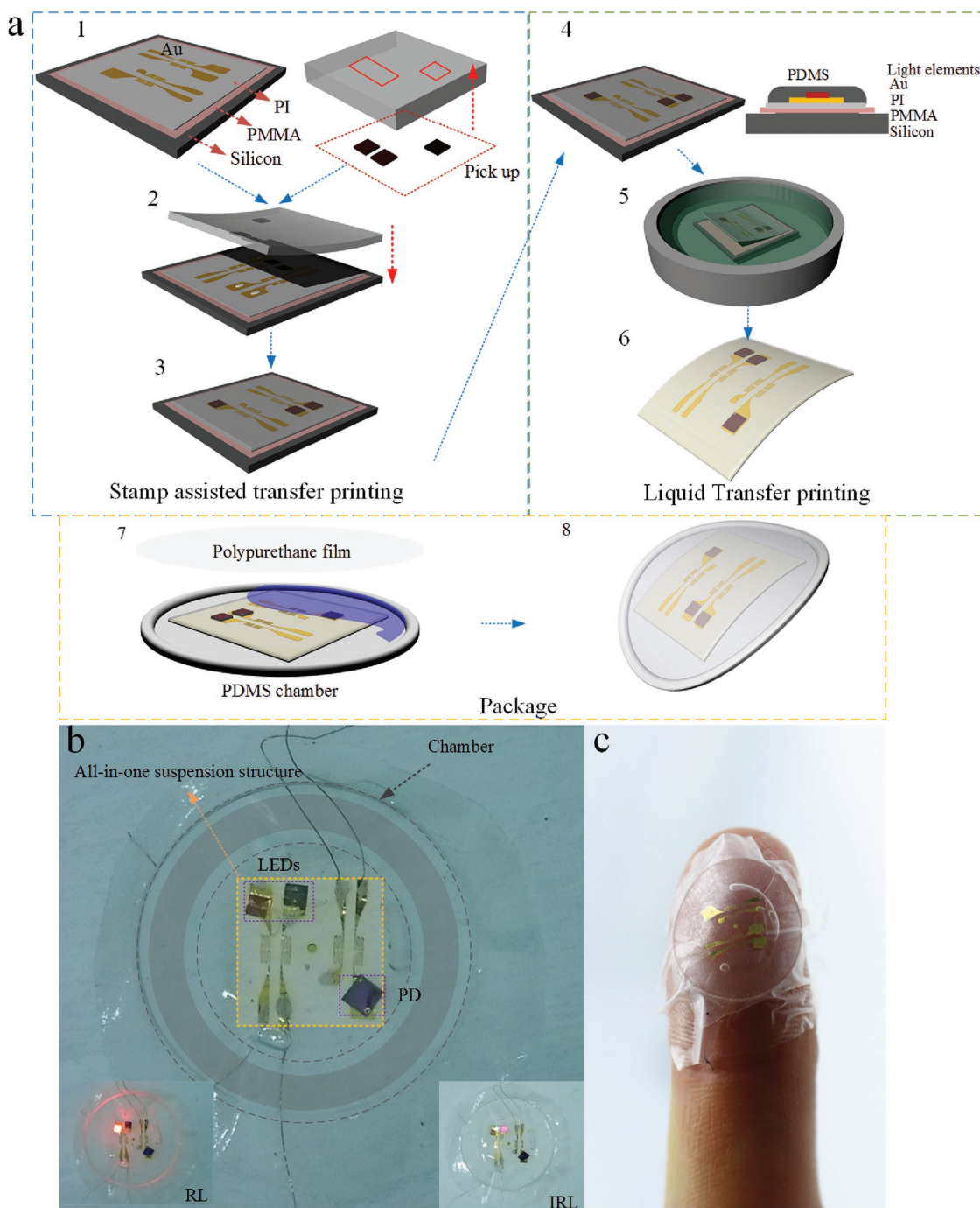


Figure 2. Fabrication and pictures of epidermal optoelectronic device via hybrid integration. a) Flowchart of fabrication steps. The key technique for involve two sequential transfer printing steps, respectively are stamp assisted for optoelectronic elements hybrid integration and liquid transfer printing for peeling off flexible island structure. b) Photographs of the integrated elements, including Au network wire with fractal shape, two light emitting elements, and one photodetector, based on GaAs and silicon material, respectively. Inset, A couple of light emitting devices turns on, the light colors are red (RL, 620 nm) and infrared (IRL, 850 nm). c) the device attached to the fingertip.

scattering in simulated tissue, and is roughly symmetry about the light source position. The relative light intensity distribution along D_{lp} on skin surface is calibrated and highlighted quantitatively in Figure 4e. The maximum reflected light appears at $D_{lp} \approx 5$ mm, and is proportional to incident light intensity. The light intensity is strongly depended on D_{lp} . The maintaining

of D_{lp} at optimal value (0.49 mm) determines stable premium light intensity signal.

To verify light path stability of the stretchable all-in-one structure, finite element method (FEM) is used to analyze the strain distribution in the island in case of tension deformation as shown in Figure 5a. The FEM results are shown in Figure 5b. In

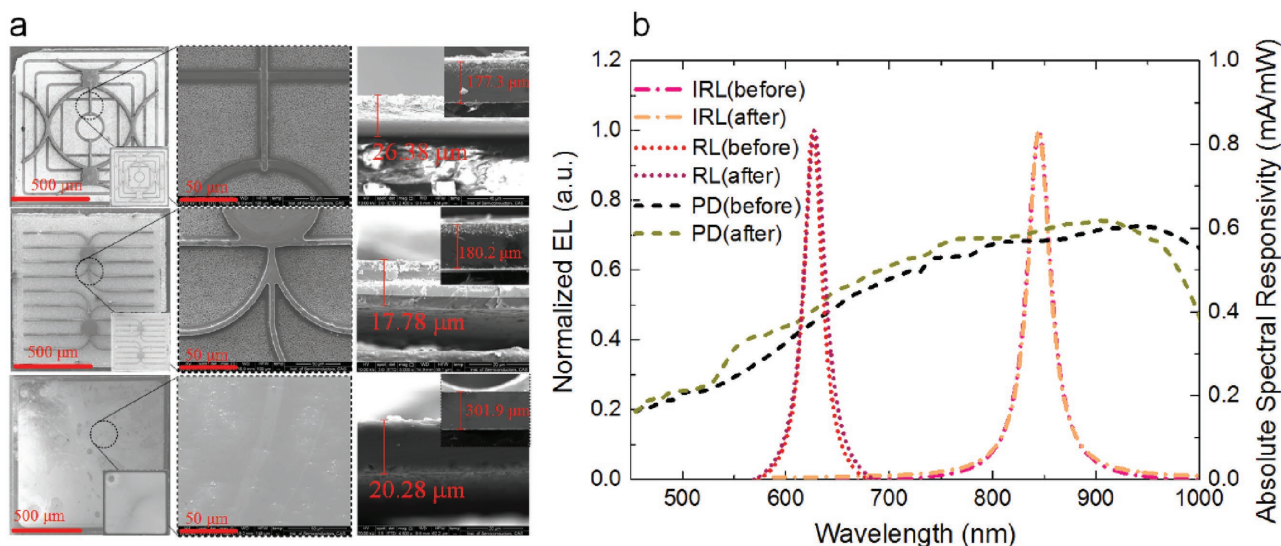


Figure 3. The property of the optoelectronic element arrays after thinning via the nanodiamond thinning process. a) The SEM photos demonstrate the morphology of the function layer surface of ultrathin red light (row first), infrared light emitting (row second) and photodetector elements (row third). The first column is the SEM images of the microstructure of the chips after thinning, in contrast to the primary chips (insets). The surface details are viewed in the second column and no crack on it after thinning process. The third column shows the thickness of the ultrathin chips with insets showing the primary chips. b) The comparison of EL spectra of LEDs and spectral responsivity of photodetector between deleting substrate and original die.

condition of maximum preloaded strain up to $\approx 40\%$, the island remains nearly unstrained as shown in the zoom-in, which indicates that the external chamber absorbs all stress and barely transmits to the internal all-in-one suspension structure. Uniaxial tension experiment is carried out to verify the effectivity

of the strain isolation structure as shown in Figure 5c. Up to $\approx 35\%$ tensile strain is loaded on the device by the home-made loading stage. Since the Au interconnects are most sensitive to the strain, its integrity is checked by microscopy as shown in the picture on the right of Figure 5c.

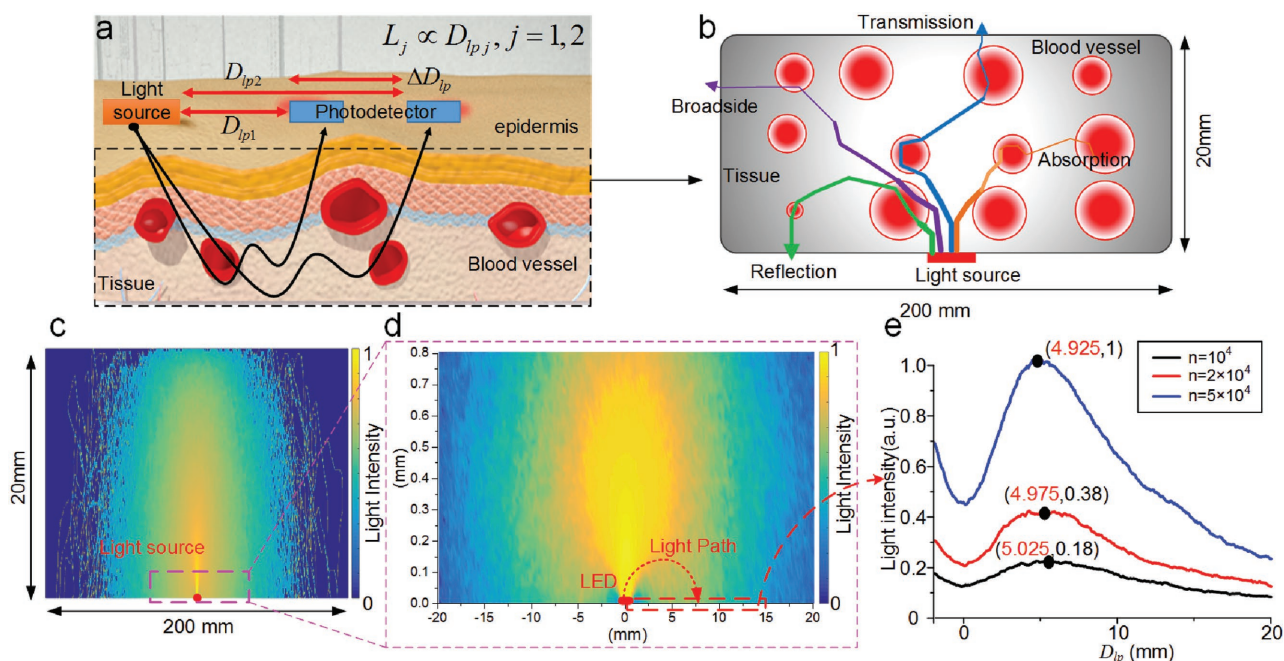


Figure 4. Model of light propagation in human tissue for optical design. a) Optical path change in human tissue caused by device deformation. D_{ip} : distance between light source and photodetector, L : optical path. b) Subcutaneous model based capillary vessel distribution of human finger and four possible light paths. c) Light distribution in the tissue with a 1 mm length light emitting element placed at middle bottom. d) Zoom-in contour of reflected light intensity distribution. e) The relationship of reflection light intensity and distance between light source and photodetector. n is the quantity of light beams.

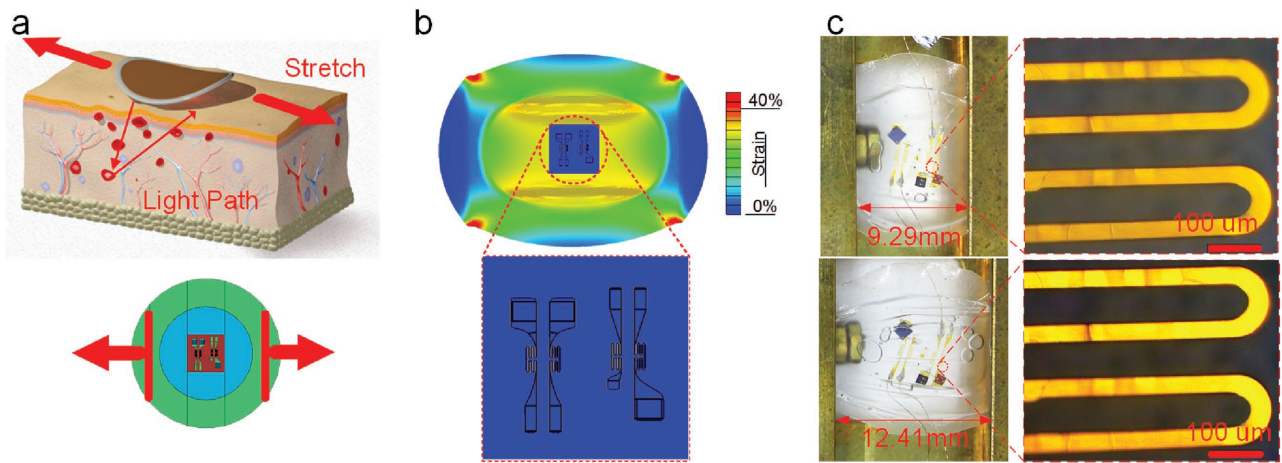


Figure 5. Mechanical property of the optoelectronic device. a) Illustration of the stretchable and flexible devices under stretching of the skin and its FEM model. b) The results of the strain isolation design demonstrated by the strain contour in case of uniaxial tension. c) Stretching test on the home-made loading stage with nominal strain up to 35% and microscopy images of the interconnect wire before and after stretching.

4. In Vitro Test

To demonstrate the practical application of the epidermal optoelectronic device, we utilize the epidermal optoelectronic device

(shown in Figure 2b) to quantitatively detect human SpO₂ and cardiac pulse rate in vitro experiment. Variable absorption parts of light under epidermis infers the message about SpO₂ and pulse rate, the generating principle is illustrated in Figure 6a,

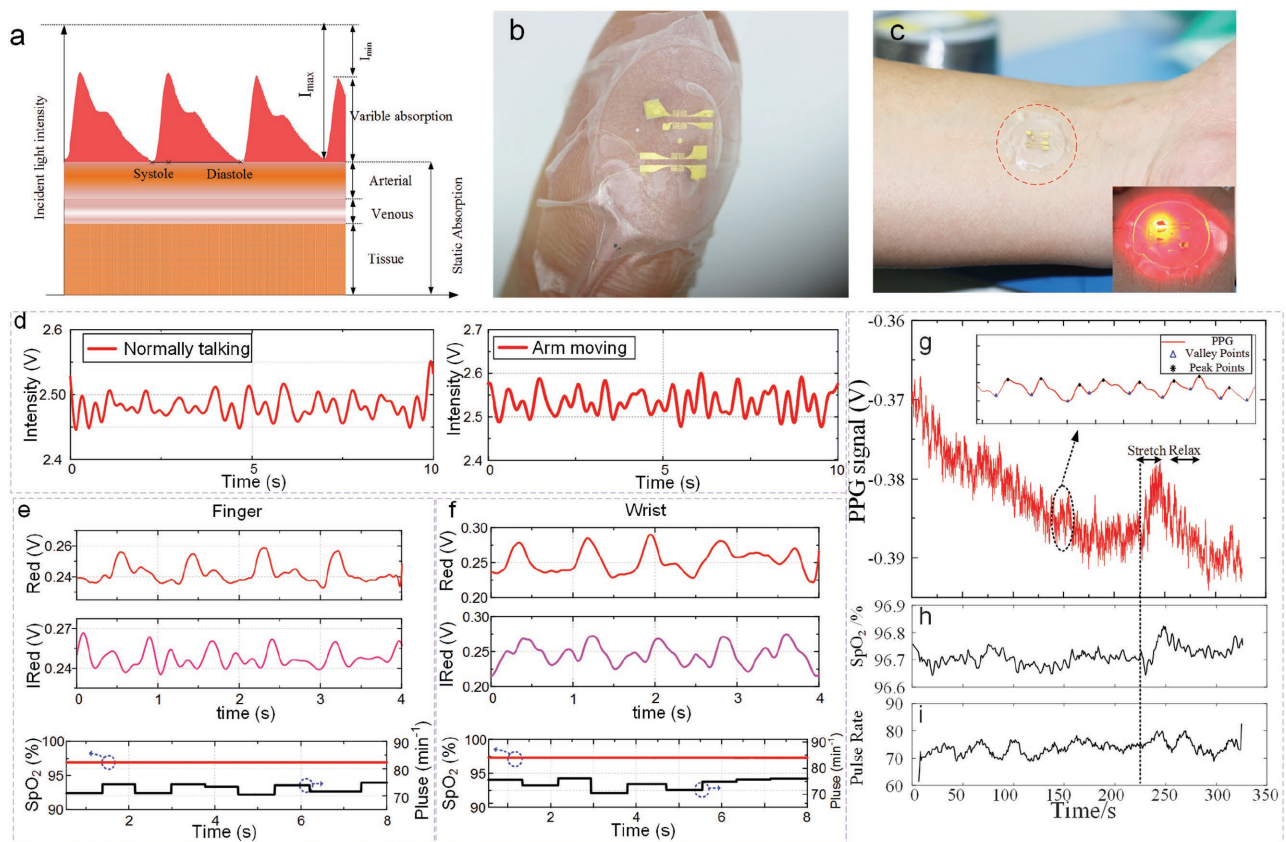


Figure 6. In vitro tests of the epidermal optoelectronic device. a) A schematic diagram of PPG signal formation by light scattering in the tissue. b) The device attached to the fingertip to measure SpO₂ and pulse rate. c) The device integrated onto the wrist with inset showing the working state of the device. d) Signal anti-disturbance test of the device on forefinger with the volunteer speaking and arm moving slowly. e, f) The SpO₂ and pulse rate measured in one period on the finger and wrist. g) PPG signal on volunteer's forehead, the stretching is caused by frown. Inset: the zoom PPG signal after filter treatment and the peak-valley points obtained for calculating SpO₂. h, i) SpO₂ and pulse rate value within 350 s monitoring.

and the analysis and deriving steps in detail are shown in the Experimental Section.

We place the epidermal optoelectronic device on the different positions, including forefinger and wrist shown in Figure 6b,c. The inset in Figure 6c shows the working state of such device on skin. To measure vital parameters precisely and accurately, we use a homemade driver (see Figure S6 in the Supporting Information) circuit to drive red and infrared light 4 s each time alternatively, and the sample rate set as 0.1 K for processing photodetector's receiving signal, including shaping-filtering and multi-stage amplification.

We test the device signal under the circumstance of volunteer speaking and forearm moving slowly, and the result is shown in Figure 6d. The volunteer normally talks and forearm moves slowly while the device is working on forefinger. Although the PPG signal distorts slightly, the regular curve still exists and can be applied for SpO₂ calculation. Finally, the SpO₂ and pulse rate is tested with a 8 s period of alternative light illumination, as shown in Figure 6e,f. The peak-to-peak time of periodic waveform reflects pulse rate, and peak-valley voltage implies the information of the SpO₂ value. Then SpO₂ is calculated with the maximum and minimum value. The probe results of heart rate and oxygen saturation were 70–75 beats per minute and 96.4%, and the parameters at wrist were 70–75 beats per minute and 97%. The data is similar on finger and wrist of a same volunteer. For directly testing the device while stretching the skin, we recalculate the SpO₂ and pulse rate. We take a strategy of pulse oximeter, which means, we use the 0.1 KHz switching time. The advantage of this strategy is a real-time SpO₂, thus we can observe the SpO₂ in the stretching processing. To avoid the disturbance caused by squeezing blood vessel while stretching, we adhere the device on volunteer's forehead, and stretching affect is produced by frown. The results are shown in Figure 6g–i. The disturbance caused by stretching change only 0.1% SpO₂, this value is completely within the acceptable range.

5. Conclusion

This study demonstrates the strategy for epidermal optoelectronic devices that can heterogeneously integrate elements based on different material. We design such devices to keep light path unchanged while the surrounding skin/tissue deforms. This approach builds on all-in-one suspension structure, which is realized by two sequential transfer printing technique. Also, nanodiamond thinning technique, with grinding millimeter size die, is utilized and 20 μm thick die is obtained. Finally, we fabricate a device as designed for SpO₂ and pulse rate measurement. As a result, this device is able to resist disturbance caused by speaking and slightly arm moving when working on the volunteer's forefinger. The proposed design, including mechanical design for flexibility and stretchability and optical design for light intensity stability, will extremely improve the performance and robustness of epidermal optoelectronic device with respect to deformation. Our strategy opens a route to manufacturing epidermal optoelectronic devices for physical measurement with exceptional versatility and potential scalability.

6. Experimental Section

Fabrication of the All-in-One Suspension Structure: a) The two steps of transfer printing for internal island structure. The fabrication process started with the preparation of films on native silicon wafer (about 1 cm × 1 cm), including PMMA/PI/Au metal (500 nm/2 μm/700 nm) sequentially. PMMA layer in the bottom acted as a sacrificial layer for liquid transfer printing, PI was the support layer and the whole conduct wire (Au), and the function devices were fabricated on the PI. The PMMA (M130002, MicroChem, USA) and PI (ZKPI-30511B, POME, CHN or PI-5), YIDUN, CHN) was spin coated and cured at the temperature of 130 °C for 2 min, 150 °C for 5 min, 90 °C for 20 min, 120 °C for 1 h, respectively. Au was deposited by sputter and etched into specific pattern with the photoresist (AZ5214E) as a mask. The Au pad was dipped by a little high purity sliver paint (05001-AB, SPI, USA) where the chips would be located. The ultrathin optoelectronic elements were carefully picked up, moved upon the specific pads by transfer printing stamp, and stuck with silver paint; the upper electrode of chips was connected to Au conductor by wire bond, which was fabricated by wire bonding. Then the PDMS (10:1 with curing agent) (184, SLYGARD, USA) was spin coated onto the Au surface with a low rotating speed (1200 rpm min⁻¹, 12 s), the thickness of PDMS was about 300 μm, and finally, PDMS was baked at a constant temperature of 65 °C for 240 min. Developing solution (diluted AZ400K, AZ electronic materials, USA) was prepared for creating liquid environment of transfer printing. The structure with silicon wafer was attached to a glass slide for attenuating break from operating. When the sacrificial layer was removed, the function layer would be floated up and cleaned by deionized water (DI) water. b) External chamber processing. The bottom half part of external packaging, which was a 500 μm thick ring shape with PDMS substrate film, was put to encapsulation molding by a pure aluminum. The above-mentioned PDMS was mixed with curing agent as proportion of 10:1, and vacuum processed for 10 min. The pure aluminum pattern which is used for modeling bottom structure was saturated in 2,2,4-trimethyl pentane (500 mL mixed with several trichloromethane droplets, 80135890, SCRC, CHN) for 30 min. The PDMS stayed quiescence in room temperature for 24 h and then spin coated onto the pattern (1200 rpm for 18 s). After being baked at a temperature of 65 °C for 4 h, PDMS was peeled off from aluminum carefully, thus the bottom and ring part were molded. The liquid PDMS was dipped and the suspension island was posited in the PDMS enclosure, the upper surface of the enclosure was polyurethane film (1624W, Tefaderm film, 3M), which stuck with the other part, and the whole device was completed.

Optoelectronic Chips Thinning: a) Thorough and fine grinding process. A little solid phenyl salicylate (PS) (30145926, SCRC, CHN) was poured onto the grinding wheel at room temperature. Then the wafer was heated to 70 °C and made to stay at that temperature until the PS was molten. Then three 3 × 3 arrays of prethinning optoelectronic devices were saturated in liquid PS, and pressed by a 10 kg weight. Then the whole bulk was put into -4 °C circumstance for about 4 h for freezing PS on wafer, as a result, the chip and grinding wheel were pasted firmly together. The extra tape and PS were scraped and cleared by a lancet. A different diameter (2.2/1.5/0.9 μm) and concentration (0.25%/0.15%/0.18%) of nano diamond grinding liquid were prepared and were responsible for rough thinning, elaborate thinning, and polishing, respectively. Also, abrasive disks with different materials, including copper, iron, and stannum, cooperated each species nano diamond liquid. The detail is seen in the Supporting information. The DI acted as a lubricant when the chips were thinning; a digital gauge was used for precisely measuring thickness during this processing. b) Optical performance testing. LEDs were tested by a fluorescence spectrometer (Princeton instruments, spectrapro2500i) and PD was detected with the response spectrum system, which was self-assembled by spectrometer (Zolix Omin λ-300) and digital lock-in Amplifiers (SRS corp, SR810).

The Model for Human Tissue and MC Simulation Method: The diameter of blood vessel was set to be in the range of 5–10 μm and distributed in a random way, according to the real human blood capillary, and the density value of the vessel was 625 per mm², all the

vessels positioned array randomly in a subcutaneous tissue whose size was 200 mm × 20 mm. A simulated light source, which was 1 mm wide, was located at the center of bottom side ejecting the light beam in random direction at effective section of 1 mm LED, as shown in inset of Figure 3b.

The substance of photon scattering disturbances was divided into two parts: (1) vessels, which acted as main absorbing and highly scattering disturbances. (2) Another tissue, the substance in creature also had ability to absorb and scatter photon. The probability of a photon to absorb and scatter was determined by $\exp(-\mu_a dr)$ and $[1 - \exp(-\mu_s dr)]$, respectively. If the photon was scattered, its new direction was calculated as follows

$$\theta_{\text{new}} = \theta_{\text{old}} + r \cos(g) \quad (1)$$

where, μ_a , μ_s , and g are absorption coefficient, scattering coefficient, and anisotropy factor respectively, r is a random number from the group. The constants of these parameters are set as in Table S1 in the Supporting Information and the NIR wavelength of 850 nm, which was also the work wavelength of oximeter device, was chosen to apply in this simulation. The path of 15 000 bundle of beam was calculated by MatLab program and photon steps dr in this simulation was 1 μm in vessel and 5 μm in another tissue.

Data Processing of the PPG Signal: Under the condition of ignoring the influence of the other substance in artery vascular and only considering hemoglobin (HbO₂) and deoxyhemoglobin (Hb), SpO₂ is defined as follows

$$\text{SpO}_2 = \frac{[\text{HbO}_2]}{[\text{HbO}_2] + [\text{Hb}]} \quad (2)$$

[HbO₂] and [Hb] represent the concentration of HbO₂ and Hb, respectively. Absorption photometry was a widely used method to measure the concentration or density of substance, that is, the concentration is proportional to transmittance or absorbance at specific wavelengths. Combined with Lambert–Beer law, the oxygen saturation is expressed as

$$\text{SpO}_2 = \frac{R \text{Ext}(\text{Hb}, \lambda_{\text{IRed}}) - \text{Ext}(\text{Hb}, \lambda_{\text{Red}})}{R(\text{Ext}(\text{Hb}, \lambda_{\text{IRed}}) - \text{Ext}(\text{HbO}_2, \lambda_{\text{IRed}})) + \text{Ext}(\text{HbO}_2, \lambda_{\text{Red}}) - \text{Ext}(\text{Hb}, \lambda_{\text{Red}})} \quad (3)$$

$\text{Ext}(\text{HbO}_2, \lambda_{\text{Red}})$, $\text{Ext}(\text{HbO}_2, \lambda_{\text{IRed}})$, $\text{Ext}(\text{Hb}, \lambda_{\text{Red}})$, $\text{Ext}(\text{Hb}, \lambda_{\text{IRed}})$ is the red and infrared light absorption coefficient of HbO₂ and Hb, respectively. R is calculated as

$$R = \ln \left[\frac{I_{\text{max}}(\lambda_{\text{Red}})}{I_{\text{min}}(\lambda_{\text{Red}})} \right] / \ln \left[\frac{I_{\text{max}}(\lambda_{\text{IRed}})}{I_{\text{min}}(\lambda_{\text{IRed}})} \right] \quad (4)$$

where, $I_{\text{max}}(\lambda_{\text{Red}})$, $I_{\text{min}}(\lambda_{\text{Red}})$, $I_{\text{max}}(\lambda_{\text{IRed}})$, and $I_{\text{min}}(\lambda_{\text{IRed}})$ is maximum and minimum light reflection intensity, respectively. Based on Equations (2) and (3), when light reflection intensity is obtained, the SpO₂ can be acquired from PPG signal.

According to spectral absorption characteristics of HbO₂/Hb (Figure 6s), in Equation (2), the following relationship existed

$$\text{Ext}(\text{Hb}, \lambda_{\text{R}}) \gg \text{Ext}(\text{HbO}_2, \lambda_{\text{R}}) \quad (5)$$

$$\text{Ext}(\text{Hb}, \lambda_{\text{IR}}) \approx \text{Ext}(\text{HbO}_2, \lambda_{\text{IR}}) \quad (6)$$

Thus, Equation (2) can be simplified as

$$\text{SpO}_2 = \frac{R \text{Ext}(\text{Hb}, \lambda_{\text{IR}}) - \text{Ext}(\text{Hb}, \lambda_{\text{R}})}{\text{Ext}(\text{HbO}_2, \lambda_{\text{R}}) - \text{Ext}(\text{Hb}, \lambda_{\text{R}})} = AR + B \quad (7)$$

Then the authors utilized commercial oximeter device to calibrate A and B ; the accurate SpO₂ was tested by the device.

Supporting Information

Supporting Information is available from the Wiley Online Library or from the author.

Acknowledgements

The authors gratefully acknowledge the support from the National Basic Research Program of China (Grant No. 2015CB351904), National Natural Science Foundation of China (Grant Nos. 11320101001, 11222220, 11227801), and Tsinghua University Initiative Scientific Research Program.

Received: September 2, 2016

Revised: December 11, 2016

Published online: February 28, 2017

- [1] J. A. Rogers, T. Someya, Y. Huang, *Science* **2010**, 327, 1603.
- [2] S. Y. Lee, K. Park, C. Huh, M. Koo, H. G. Yoo, S. Kim, C. S. Ah, G. Y. Sung, K. J. Lee, *Nano Energy* **2012**, 1, 1.
- [3] M. Drack, I. Graz, T. Sekitani, T. Someya, M. Kaltenbrunner, S. Bauer, *Adv. Mater.* **2015**, 27, 1.
- [4] R. H. Kim, D. H. Kim, J. Xiao, B. H. Kim, S. I. Park, B. Panilaitis, R. Ghaffari, J. Yao, M. Li, Z. Liu, V. Malyarchuk, D. G. Kim, A. P. Le, R. G. Nuzzo, D. L. Kaplan, F. G. Omenetto, Y. Huang, Z. Kang, J. A. Rogers, *Nat. Mater.* **2010**, 9, 929.
- [5] S. I. Park, D. S. Brenner, G. Shin, C. D. Morgan, B. A. Copits, H. U. Chung, M. Y. Pullen, K. N. Noh, S. Davidson, S. J. Oh, J. Yoon, K. I. Jang, V. K. Saminen, M. Norman, J. G. Grajales-Reyes, S. K. Vogt, S. S. Sundaram, K. M. Wilson, J. S. Ha, R. Xu, T. Pan, T. I. Kim, Y. Huang, M. C. Montana, J. P. Golden, M. R. Bruchas, R. W. Gereau, J. A. Rogers, *Nat. Biotechnol.* **2015**, 33, 1280.
- [6] Y. Sun, W. M. Choi, H. Jiang, Y. Y. Huang, J. A. Rogers, *Nat. Nanotechnol.* **2006**, 1, 201.
- [7] Y. Chen, B. Lu, Y. Chen, X. Feng, *IEEE Electron Device Lett.* **2016**, 37, 496.
- [8] D. H. Kim, N. Lu, R. Ma, Y. S. Kim, R. H. Kim, S. Wang, J. Wu, S. M. Won, H. Tao, A. Islam, K. J. Yu, T. I. Kim, R. Chowdhury, M. Ying, L. Xu, M. Li, H. J. Chung, H. Keum, M. McCormick, P. Liu, Y. W. Zhang, F. G. Omenetto, Y. Huang, T. Coleman, J. A. Rogers, *Science* **2011**, 333, 838.
- [9] M. Jamal, S. S. Kadam, R. Xiao, F. Jivan, T. Onn, R. Fernandes, T. D. Nguyen, D. H. Gracias, *Adv. Healthcare Mater.* **2013**, 2, 8.
- [10] P. J. Chowienzyk, R. P. Kelly, H. MacCallum, S. C. Millasseau, T. L. G. Andersson, R. G. Gosling, J. M. Ritter, E. E. Ånggård, *J. Am. Coll. Cardiol.* **1999**, 34, 2007.
- [11] Y. Sun, W. M. Choi, H. Jiang, Y. Y. Huang, J. A. Rogers, *Nat. Nanotechnol.* **2006**, 1, 201.
- [12] K. Tae-il, K. Rak-Hwan, J. A. Rogers, *IEEE Photonics J.* **2012**, 4, 607.
- [13] W. Gao, S. Emaminejad, H. Y. Nyein, S. Challa, K. Chen, A. Peck, H. M. Fahad, H. Ota, H. Shiraki, D. Kiriya, D. H. Lien, G. A. Brooks, R. W. Davis, A. Javey, *Nature* **2016**, 529, 509.
- [14] R. C. Webb, A. P. Bonifas, A. Behnaz, Y. Zhang, K. J. Yu, H. Cheng, M. Shi, Z. Bian, Z. Liu, Y. S. Kim, W. H. Yeo, J. S. Park, J. Song, Y. Li, Y. Huang, A. M. Gorbach, J. A. Rogers, *Nat. Mater.* **2013**, 12, 938.
- [15] J. Kim, G. A. Salvatore, H. Araki, A. M. Chiarelli, Z. Xie, A. Banks, X. Sheng, Y. Liu, J. W. Lee, K. Jang, S. Y. Heo, K. Cho, H. Luo, B. Zimmerman, J. Kim, L. Yan, X. Feng, S. Xu, M. Fabiani, G. Gratton, Y. Huang, U. Paik, J. A. Rogers, *Sci. Adv.* **2016**, 2, 8.
- [16] J. Kim, P. Gutruf, A. M. Chiarelli, S. Y. Heo, K. Cho, Z. Xie, A. Banks, S. Han, K. Jang, J. W. Lee, K. Lee, X. Feng, Y. Huang, M. Fabiani, G. Gratton, U. Paik, J. A. Rogers, *Adv. Funct. Mater.* **2016**.

- [17] M. Hammer, S. Leistriz, L. Leistriz, D. Schweitzer, *IEEE Trans. Biomed. Eng.* **2001**, *48*, 592.
- [18] M. S. White, M. Kaltenbrunner, E. D. Głowacki, K. Gutnichenko, G. Kettlgruber, I. Graz, S. Aazou, C. Ulbricht, D. A. M. Egbe, M. C. Miron, Z. Major, M. C. Scharber, T. Sekitani, T. Someya, S. Bauer, N. S. Sariciftci, *Nat. Photonics* **2013**, *7*, 811.
- [19] Y. Diao, Y. Zhou, T. Kurosawa, L. Shaw, C. Wang, S. Park, Y. Guo, J. A. Reinspach, K. Gu, X. Gu, B. C. Tee, C. Pang, H. Yan, D. Zhao, M. F. Toney, S. C. Mannsfeld, Z. Bao, *Nat. Commun.* **2015**, *6*, 7955.
- [20] P. Chen, K. Xu, X. Li, Y. Guo, D. Zhou, J. Zhao, X. Wu, C. Wu, Y. Xie, *Chem. Sci.* **2014**, *5*, 2251.
- [21] B. Lu, Y. Chen, D. Ou, H. Chen, L. Diao, W. Zhang, J. Zheng, W. Ma, L. Sun, X. Feng, *Sci. Rep.* **2015**, *5*, 16065.
- [22] W. Zhou, Z. Ma, S. Chuwongin, Y.-C. Shuai, J.-H. Seo, D. Zhao, H. Yang, W. Yang, *Opt. Quantum Electron.* **2012**, *44*, 605.
- [23] L. Pan, A. Chortos, G. Yu, Y. Wang, S. Isaacson, R. Allen, Y. Shi, R. Dauskardt, Z. Bao, *Nat. Commun.* **2014**, *5*, 3002.
- [24] S. Gong, W. Schwalb, Y. Wang, Y. Chen, Y. Tang, J. Si, B. Shirinzadeh, W. Cheng, *Nat. Commun.* **2014**, *5*, 3132.
- [25] Y. Chen, B. Lu, Y. Chen, X. Feng, *IEEE Electron Device Lett.* **2016**, *37*, 4.
- [26] E. Okada, M. Firbank, M. Schweiger, S. R. Arridge, M. Cope, D. T. Delpy, *Appl. Opt.* **1997**, *36*, 21.
- [27] D. J. Faber, M. C. G. Aalders, E. G. Mik, B. A. Hooper, M. J. C. van Gemert, T. G. van Leeuwen, *Phys. Rev. Lett.* **2004**, *93*, 2.
- [28] H. Duadi, D. Fixler, R. Popovtzer, *J. Biomed. Opt.* **2013**, *18*, 111408.